Title

Genetic Algorithm Optimization of a Finned-Tube Heat Exchanger Modeled With Volume-Averaging Theory

Journal

Journal of Heat Transfer, 135(8)

ISSN

0022-1481

Authors

Geb, David
Zhou, Feng
DeMoulin, George
et al.

Publication Date

2013-07-18

DOI

10.1115/1.4024091

Peer reviewed

Genetic Algorithm Optimization of a Finned-Tube Heat Exchanger Modeled With Volume-Averaging Theory

David Geb[1]
e-mail: dvdgb15@ucla.edu

Feng Zhou

George DeMoulin

Ivan Catton

Morrin-Gier-Martinelli Heat Transfer Memorial Laboratory,
Department of Mechanical and Aerospace Engineering,
School of Engineering and Applied Science,
University of California,
Los Angeles, 48-121 Engineering IV,
420 Westwood Plaza,
Los Angeles, CA 90095-1597

This paper proposes and implements a new methodology for optimizing finned-tube heat exchangers (FTHEs) using a volume-averaging theory (VAT) hierarchical physical model and a genetic algorithm (GA) numerical optimizer. This method allows for multiple-parameter constrained optimization of FTHEs by design of their basic morphological structures. A consistent model is used to describe transport phenomena in a FTHE based on VAT, which allows for the volume-averaged conservation of mass, momentum, and energy equations to be solved point by point, with the morphology of the structure directly incorporated into the field equations and full conjugate effects included. The equations differ from those often presented in porous media modeling and are developed using a rigorous averaging technique, hierarchical modeling methodology, and fully turbulent models with Reynolds stresses and fluxes in every pore space. These averaged equations have additional integral and differential terms that must be dealt with in order for the equation set to be closed, and recent work has provided this closure for FTHEs. The resulting governing equation set is relatively simple and is discretized and quickly solved numerically. Such a computational solution algorithm is fast running, but still able to present a detailed picture of the temperature fields in both of the fluid flows as well as in the solid structure of the heat exchanger. A GA is integrated with the VAT-based solver to carry out the FTHE numerical optimization, which is a ten parameter problem, and the FTHE is optimized subject to imposed constraints. This method of using the VAT-based solver fully integrated with a GA optimizer results in a new all-in-one tool for performing multiple-parameter constrained optimization on FTHEs.
[DOI: 10.1115/1.4024091]

Keywords: volume averaging theory, genetic algorithm, optimization, finned-tube heat exchanger, conjugate heat transfer, hierarchical modeling, porous media

Introduction

Despite the crucial role of heat exchangers in industrial installations, there is still a great deal of empiricism in their design. Although current guidelines provide an ad hoc solution, a unified design approach based on simultaneous modeling of the thermal hydraulics and thermal structural behavior has not been proposed beyond direct numerical simulation-based methods, which at this point are too computationally costly for designers. As a consequence, designs are often overly constrained with a resulting economic penalty. It is apparent that a more scientific procedure for the design and optimization of heat exchangers is needed.

Past work, while using GAs for multiparameter optimization, has relied upon traditional methods of heat exchanger thermal modeling. In one such study, Ozkol and Komurgoz [1] optimized the size of a heat exchanger for a given surface with the help of a GA. They used the number of transfer units (ε-NTU) method and sought to minimize cost. Similarly, Xie et al. [2] applied a GA to optimize FTHEs using the log-mean temperature difference (LMTD) method for the thermal design and imposed pressure drop constraints. Experimental transfer coefficient correlations were employed for both the air and water sides, and the total weight and annual cost of the FTHE were minimized separately. In a more detailed study, Domanski [3] describes a public domain FTHE simulation software tool, EVAP-COND, a study continued in Ref. [4], and discusses its integration with an optimization routine in Ref. [5]. The heat exchanger performance is determined using a tube-by-tube segmented LMTD approach with empirical correlations employed for the heat transfer coefficients and pressure drops. Similarly, Jiang et al. [6] describe a flexible design tool, CoilDesigner, that can also be integrated with optimization procedures [7], adopt a network viewpoint, and take a segmented modeling approach using the ε-NTU method.

Other investigators have employed direct numerical simulation–based methods coupled with GAs. Mousavi et al. [8], for example, used a GA to optimize the structure of a finned channel for a fixed flow rate in terms of the location and size of the fins with the aim of minimizing pressure drop and maximizing heat transfer. The fluid flow and temperature fields were obtained using the finite volume method, assuming two-dimensional, laminar, steady-state flow with constant properties [9]. The GA found an optimum configuration; however, in this study, the fins were considered perfectly conductive and of negligible thickness, so the solid side was not treated and the conjugate problem was not solved.

Although not employing a GA, Matos et al. [10] demonstrated what they labeled as "numerical and experimental double optimization" on the geometry of staggered circular and elliptical finned tubes. Their objective was to find the optimal geometry in terms of tube-to-tube spacing, tube eccentricity, and fin-to-fin

[1]Corresponding author.

Contributed by the Heat Transfer Division of ASME for publication in the Journal of Heat Transfer. Manuscript received July 22, 2012; final manuscript received March 18, 2013; published online July 18, 2013. Assoc. Editor: Giulio Lorenzini.

spacing, such that the volumetric heat transfer density was maximized, subject to a volume constraint. Assuming incompressible, steady state, laminar flow with constant properties, three-dimensional direct numerical calculations of the flow and temperature were performed using the finite element method. The numerical calculations were experimentally validated and used to perform the parametric optimization. Unfortunately, it is apparent that the cost of the direct numerical simulations and/or experimental trials prevented the possibility of a more thorough search of the domain, and only four eccentricities, four tube pitches, and two flow rates were considered (the number of fin-to-fin spacings considered was not reported).

In a good example of properly accounting for the conjugate effects, Fabbri [11] considered heat transfer into a channel flow through a wall with a corrugated surface whose profile is periodic and described by a fifth order polynomial. A finite element model solved the conjugate heat transfer problem assuming two-dimensional, laminar, steady-state, fully developed, incompressible flow with uniform properties. Optimal corrugation profiles were obtained with a GA by maximizing the heat transfer for a given channel pressure drop and wall volume for two distinct Reynolds and Prandtl numbers. However, although the number of simulations was not reported, it is expected that the computational costs significantly limited the search ability of the GA.

Foli et al. [12] used a multiobjective GA to optimize the performance of a micro heat exchanger by considering the shape of its channels. They simultaneously maximized the heat transfer and minimized the pressure drop by searching for the optimal shape of the separator between the fluids, which was represented by two nonuniform rational B-splines (NURBS) with ten control points. The governing flow and heat transfer equations were solved with commercially available computational fluid dynamics (CFD) software, and conjugate heat transfer effects between the solid and fluid were taken into account. A Pareto optimal front (i.e., the set of all nondominated solutions) was obtained; however, it was reported that a month of calculations were necessary to do so.

In yet another example of the significant costs of using CFD for heat exchanger optimization, a multiobjective GA optimization on the tube shape in a tube bank heat exchanger using direct numerical simulation was detailed by Hilbert et al. [13]. A steady, two-dimensional, laminar flow model was employed, and the tube-side flow and heat transfer were ignored. The tube shape was varied by adjusting four parameters that described it. The objectives were to simultaneously maximize the heat transfer while minimizing the pressure loss. A fully automatic optimization computer package would repeatedly call special software to generate both the tube geometry from input parameters and the appropriate simulation mesh and the CFD program to perform the numerical simulation over the mesh. Postprocessing of the CFD results to obtain the objective function values was done with an in-house interfacing code. The simulations were performed in parallel on a multinode Linux personal computer (PC) cluster with 15 worker PCs, and the population of the GA was 30 and it operated for 20 generations. Solution times on the order of 10 min and a Pareto optimal front were reported.

Although they did not consider optimization, Hooman and Gurgenci [14] adopted a porous medium approach to *turbulent* transport in air flow over a finned-tube bundle and considered the effects of fin height and number density variations. Using a commercial CFD package that solves porous media turbulent transport equations, given the porosity, permeability, and a form drag coefficient, they considered two-dimensional, steady-state, turbulent transport over the finned-tube bundle represented as a porous medium. Once the porous media model was calibrated against experimental data, it yielded reliable thermal predictions. The governing equations used in Ref. [14], however, were developed from ad hoc considerations and not a rigorous mathematical formulation, and the heterogeneous structure of the finned-tube bundle was homogenized.

The VAT model that is used in the present study to optimize the thermal hydraulic characteristics of FTHEs addresses many of the undesirable characteristics of the methods discussed above. As will be explained, its ability to directly incorporate the morphology description and quickly yield a nonlocal description of the temperature and flow fields in the hierarchical and heterogeneous device based on strictly derived mathematical statements, with full conjugate effects and turbulence modeling included, makes it an ideal tool for heat exchanger optimization. The ten-parameter genetic algorithm (GA) optimization study starts with the developed VAT transport model for FTHEs. This model is the basis for an optimization method that enables full exploitation of the possible parameter variations that are known to be beneficial to the heat exchanger performance. With the use of VAT, heat exchanger modeling and optimization are based on theoretically correct governing field equations rather than the usual balance equations or the semiempirical porous media models. Before initiating the optimization procedure, what is to be optimized must be determined and the constraints must be set from physical and specified limitations. Presently, in this work, this is done somewhat arbitrarily, due to the fact that different designers will have different objectives, so the present case study is meant to serve as a demonstration. Nonetheless, the method presented is general and may be easily adapted to the particular needs of individual designers.

VAT Model

Previous work has shown that flow and heat transfer in heat exchangers can be treated as phenomena in highly heterogeneous structures and that their behavior can be properly predicted with porous media modeling through applying volume-averaging theory (VAT) to the Navier–Stokes and thermal energy equations for both the fluid and solid phases [15,16]. Derivation of the VAT-based equations governing momentum and heat transport in such media is based on averaging the transport equations in both the fluid and solid phases of the heterogeneous medium over a certain representative elementary volume (REV) (see, for example, Whitaker [17–19] for laminar regime developments and Shcherban et al. [20], Primak et al. [21], Travkin and Catton [22], and Travkin et al. [23] for turbulent regime developments). Such VAT-based modeling directly incorporates the medium morphology characteristics into the governing field equations. Using different flow regime transport models and second order turbulence models, equation sets are obtained for turbulent momentum transport and *three*-temperature heat transport in heterogeneous heat exchanger media while accounting for interphase exchange. The equations differ from those often presented in the literature and were developed using an advanced averaging technique, a hierarchical modeling methodology, and fully turbulent models. Independent treatment of turbulent energy transport in the fluid phase and energy transport in the solid phase connected through the interfacial surface allows for more accurate modeling of the heat transfer mechanisms between heterogeneous structures and the fluid phases, and if one is to perform a geometric optimization, one must separate convection effects from conduction effects and solve a conjugate problem, as is done in the present VAT model.

The VAT-based model for hierarchical and heterogeneous media that is presented allows for the representation of a finned-tube heat exchanger (FTHE) (Fig. 1). VAT allows a FTHE to be analyzed as a multilevel device and results in a nonlocal description of its hierarchical, multiscaled transport processes. The lowest level is the fluid-solid interface, where the transport coefficients are determined. The next level up in the hierarchy is the local fluid-solid interaction, which is a conjugate problem with the heat transfer and drag coefficients acting as the connections between the solid and fluid. The uppermost level concerns the overall behavior of the device, on which the GA optimization study operates. The VAT model lends itself to a hierarchical and heterogeneous analysis of a FTHE in a rigorous way, allowing the

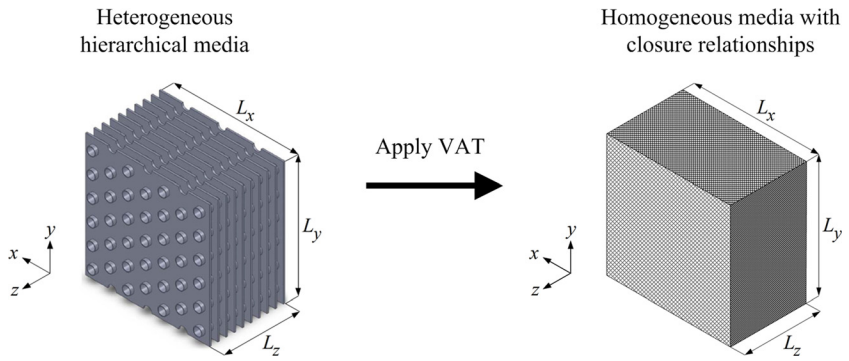

Fig. 1 VAT-based porous media model of a FTHE

effect of the lowest level, the inner passage way surfaces, to impact the uppermost scale, the overall heat exchanger performance, all while including the full conjugate effects. Its unique ability to allow a combination of direct general physical and mathematical statements with the convenience of segmented analysis, whereby overall physical processes or groups of phenomena are divided into selected subprocesses or phenomena that are interconnected, each to the others, by an adopted chain or set of dependencies usually employed in heat exchanger design, makes it an attractive tool.

In the present model, both the fin-side and tube-side flows are considered as separate "porous flows." Air is the fin-side gas, water is the tube-side liquid, and the exchanger is steel. The VAT-based momentum equation for the fin side is

$$-\frac{1}{\rho_1}\frac{\partial\langle\bar{p}_1\rangle_f}{\partial x}+\frac{\partial}{\partial z}\left(\langle m_1\rangle(\tilde{\nu}_{T_1}+\nu_1)\frac{\partial\tilde{\bar{u}}_1}{\partial z}\right)+c_{d_1}S_{w_1}\frac{\tilde{\bar{u}}_1^2}{2}=0 \quad (1)$$

and that for the tube side is

$$-\frac{1}{\rho_2}\frac{\partial\langle\bar{p}_2\rangle_f}{\partial z}+\frac{\partial}{\partial x}\left(\langle m_2\rangle(\tilde{\nu}_{T_2}+\nu_2)\frac{\partial\tilde{\bar{w}}_2}{\partial x}\right)+c_{d_2}S_{w_2}\frac{\tilde{\bar{w}}_2^2}{2}=0 \quad (2)$$

A discussion on the evaluation of $\tilde{\nu}_T$ in Eqs. (1) and (2) is presented in previous papers [15,16].

While the air flows straight through the exchanger in the positive x direction, the water follows an oscillatory path through the exchanger (Fig. 2). Such an oscillatory flow path is modeled as N_x porous channel flows of cross-stream width L_x/N_x, alternating in the positive and negative z directions. As the water exits the exchanger on one side, it adiabatically returns through the tube bend with pressure drop neglected in the tube bend here for simplicity.

Because we are dealing with a conjugate heat transfer problem, the thermal energy equations for the solid and *both* fluid phases are required. For the fin-side fluid, the VAT-based thermal energy equation is written as

$$\langle m_1\rangle\rho_1\tilde{\bar{u}}_1c_{p_1}\frac{\partial\tilde{\bar{T}}_1}{\partial x}=h_1S_{w_1}\left(\tilde{T}_s-\tilde{\bar{T}}_1\right) \quad (3)$$

and for the tube-side fluid it is written as

$$\langle m_2\rangle\rho_2\tilde{\bar{w}}_2c_{p_2}\frac{\partial\tilde{\bar{T}}_2}{\partial z}=h_2S_{w_2}\left(\tilde{T}_s-\tilde{\bar{T}}_2\right) \quad (4)$$

For the solid phase, the VAT-based thermal energy equation is written as

$$\frac{\partial}{\partial x}\left[(1-\langle m_1\rangle-\langle m_2\rangle)k_s\frac{\partial\tilde{T}_s}{\partial x}\right]+\frac{\partial}{\partial z}\left[(1-\langle m_1\rangle-\langle m_2\rangle)k_s\frac{\partial\tilde{T}_s}{\partial z}\right]=h_1S_{w_1}\left(\tilde{T}_s-\tilde{\bar{T}}_1\right)+h_2S_{w_2}\left(\tilde{T}_s-\tilde{\bar{T}}_2\right) \quad (5)$$

Closure of the general VAT-based integrodifferential equations relies on the determination of four terms. These terms are locally averaged over each REV in the domain and are the specific surface area of the fluid-solid interface, S_w, the porosity, or the volume of the fluid divided by the total volume, $\langle m\rangle$, and the momentum and heat transport coefficients, c_d and h, respectively.

The local porosity and specific surface area are determined directly by the specified morphology of the engineered porous media structure. The REV, over which they are defined for the case of a FTHE, is depicted in Fig. 3. The porosity for the fin-side of the FTHE is written as

$$\langle m_1\rangle=1-\frac{\delta_f}{F_p}-\frac{\pi D_c^2(F_p-\delta_f)}{4P_xP_yF_p} \quad (6)$$

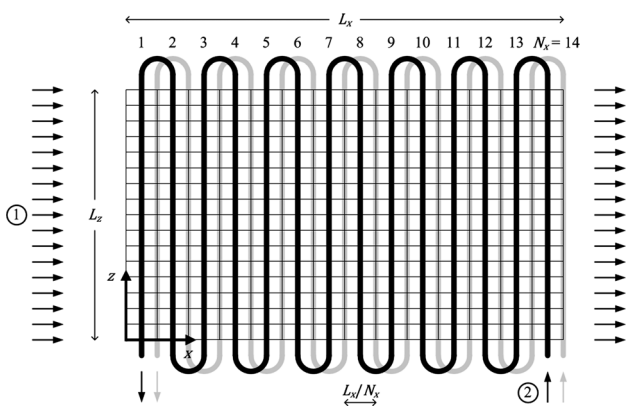

Fig. 2 Schematic of computational grid and coil circuitry

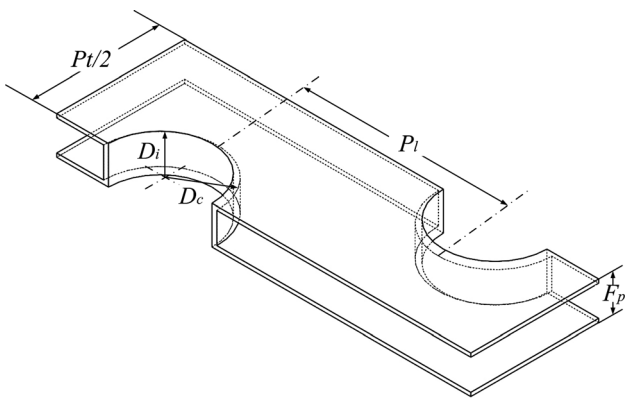

Fig. 3 Representative elementary volume (REV) for a finned-tube heat exchanger [25]

and that for the tube-side is written as

$$\langle m_2 \rangle = \frac{\pi D_i^2}{4 P_x P_y} \tag{7}$$

The specific surface area for the fin-side is given by

$$S_{w_1} = \frac{2P_xP_y - 2\pi\left(\frac{D_c}{2}\right)^2 + \pi D_c\left(F_p - \delta_f\right)}{P_xP_yF_p} \tag{8}$$

and that for the tube-side is given by

$$S_{w_2} = \frac{\pi D_i}{P_x P_y} \tag{9}$$

The local interfacial transport coefficients, c_d and h, are also needed to close the VAT-based governing equations, and clear definitions of these terms were rigorously derived from the lower-scale Navier–Stokes and thermal energy equations by Travkin and Catton [16]. The drag coefficient c_d has the general form

$$c_d = 2\frac{\int_{\partial S_w} \bar{p}\cdot d\vec{s}}{\rho_f \tilde{\tilde{u}}^2 A_{wp}} \cdot \frac{S_{wp}}{S_w} + 2\frac{\int_{\partial S_w} \tau_{wL}\cdot d\vec{s}}{\rho_f \tilde{\tilde{u}}^2 A_w} + 2\frac{\int_{\partial S_w} \tau_{wT}\cdot d\vec{s}}{\rho_f \tilde{\tilde{u}}^2 A_w} - \frac{\frac{\partial}{\partial x_j}\langle \hat{\tilde{u}}_i \hat{\tilde{u}}_j \rangle_f}{\frac{1}{2}\rho \tilde{\tilde{u}}^2} + \frac{\frac{\partial}{\partial x_j}\left(\left\langle \tilde{\nu}_T \frac{\partial \tilde{\tilde{u}}_i}{\partial x_j}\right\rangle_f\right)}{\frac{1}{2}\rho \tilde{\tilde{u}}^2} \tag{10}$$

and the heat transfer coefficient h has the general form

$$h = \frac{\frac{1}{\Delta\Omega}\int_{\partial S_w}\left(k_f + k_T\right)\nabla T_f \cdot d\vec{s} - \rho_f c_{p_f}\nabla\cdot\left(\langle m\rangle\left\{-\hat{\tilde{u}}\hat{\tilde{T}}_f\right\}_f\right) + \nabla\cdot\left(\frac{k_f}{\Delta\Omega}\int_{\partial S_w} T_f d\vec{s}\right)}{S_w\left(\tilde{T}_s - \tilde{\tilde{T}}_f\right)} \tag{11}$$

Collecting published experimental measurements of friction factor and heat transfer performance for the fin-side of FTHEs from Wang et al. [24], Zhou et al. [25] rescaled the data using a length scale derived from VAT and obtained simple correlations for the fin-side drag and heat transfer coefficients. The drag coefficient, Eq. (10), is related to the friction factor and, for the fin-side, is

$$c_{d_1} \approx f_1 = \frac{112.4}{\mathrm{Re}_1} + 0.252 \tag{12}$$

Similarly, the Nusselt number on the fin-side is expressed as

$$\mathrm{Nu}_1 = 0.24\,\mathrm{Re}_1^{0.6}\mathrm{Pr}^{1/3} \tag{13}$$

For closure of the tube side, all the scaling factors are equal to one (i.e., $D_{h_2} = D_i$), and the friction factor and Nusselt number correlations for fully developed flow in a pipe are applicable for closure of the tube-side VAT equations. Techo et al. [26] correlated the friction factor for turbulent pipe flow as

$$c_{d_2} \approx f_2 = \left\{1.7372\ln\left[\frac{\mathrm{Re}_2}{1.964\ln(\mathrm{Re}_2) - 3.8215}\right]\right\}^{-2} \tag{14}$$

As for the heat transfer coefficient, h_2, Whitaker [27] showed that the experimental data for Nusselt number from a number of investigators for turbulent pipe flow is nicely correlated by the expression

$$\mathrm{Nu}_2 = 0.015\,\mathrm{Re}_2^{0.83}\mathrm{Pr}^{0.42} \tag{15}$$

At this point in the analysis, the VAT-based model of FTHEs, Eqs. (1)–(5), is fully closed by Eqs. (6)–(9) and (12)–(15). With the closure expressions determined, the governing equation set is relatively simple and is numerically solved on a modern laptop in just seconds to yield a nonlocal description of the physical fields, thus opening the door to thorough optimization studies based on full simulations. The details of the computational procedure used to solve the VAT-based governing equations were provided in Ref. [15] and constant physical properties are assumed in this study. The proper grid size needed to obtain grid-independent results with a uniform grid for several selected cases was established and then dynamically adjusted in proportion to the domain size (i.e., L_x and L_z) throughout the optimization procedure. Moreover, only one row of tubes in the y direction was considered for this case, as symmetry allows the heat exchanger capability to be increased by increasing the number of rows in the y direction.

Genetic Algorithm Optimization

A basic genetic algorithm (GA) is employed to perform the multiple (10)-parameter constrained optimization on a plain finned-tube heat exchanger (FTHE). The fitness function associated with the FTHE, $F(\mathbf{x})$, is chosen to be

$$F(\mathbf{x}) = \varepsilon = \dot{Q}_1/\dot{Q}_{\max} \tag{16}$$

(i.e., the heat exchanger effectiveness). This fitness function is to be maximized over the bounded $n = 10$-dimensional search space,

$$\mathbf{x} \equiv \left(D, \delta_d, S_x, S_y, N_x, N_y, \delta_f, S_z, L_z, \dot{m}_1\right) \tag{17}$$

where the parameters are bounded between minimum and maximum values, $\mathbf{x}_{\min}$ and $\mathbf{x}_{\max}$, respectively, as shown in Table 1. Although designers often find themselves selecting some of these parameters (e.g., D, δ_d, δ_f) discretely from standard tables found in handbooks or production manuals, we have chosen to consider them as continuous variables so as not to restrict the study to a particular set of possible values. If one wants to consider a

Table 1 Search parameters and their ranges

$\mathbf{x}$	$\mathbf{x}_{\min}$	$\mathbf{x}_{\max}$
D (mm)	5.00	20.00
δ_d (mm)	1.00	5.00
S_x	1.00	5.00
S_y	0.50	2.50
N_x	1	50
N_y	1	50
δ_f (mm)	0.50	10.00
S_z	1.00	10.00
L_z (mm)	50.00	1500.00
$\dot{m}_1$ (kg s^{-1})	1.00	40.00

Table 2 Physical and optimization constraints

Physical constraints	
$D - 2\delta_d \geq 1$ mm	(20)
$\sqrt{P_x^2/4 + P_y^2} - D \geq 1$ mm	(21)
$P_x - D \geq 1$ mm	(22)
$2P_y - D \geq 1$ mm	(23)
$F_p - \delta_f \geq 1$ mm	(24)
Optimization constraints	
$PP_T \leq 60$ kW	(25)
$W \leq 300$ kg	(26)

discrete set of possible values for these variables, it is simple to adapt the present method to do so. The mass flow rate of the hot water, $\dot{m}_2$, along with the inlet temperatures of the air, $\tilde{\tilde{T}}_{1,\text{in}}$, and water, $\tilde{\tilde{T}}_{2,\text{in}}$, are taken to be set values in this study at

$$\dot{m}_2 = 1.0 \text{ kg s}^{-1}, \quad \tilde{\tilde{T}}_{1,\text{in}} = 30\,^\circ\text{C}, \quad \text{and} \quad \tilde{\tilde{T}}_{2,\text{in}} = 60\,^\circ\text{C} \quad (18)$$

It is obvious that physical constraints on the search space should be implemented when performing the numerical optimization. The physical constraints used here are tabulated in Table 2 and can be visualized in Fig. 4. Additionally, several optimization constraints are chosen to be implemented. These constraints are also tabulated in Table 2 and, in general, are selected by the designer for a given objective.

As the GA optimization routine commences, an initial population of FTHEs is generated by creating N_P individuals with randomly chosen values for each of their bounded n parameters. The fitness of each of these individuals is then determined, and the evolutionary process may begin. The population size N_P remains fixed throughout the evolutionary process, spanning N_G generations. During each generation, offspring are produced and stored until N_P children have been created. Subsequently, the parent population is exterminated and replaced by the child population. Elitism is enforced so that the fittest individual in the population will survive and be passed into the next generation.

The reproductive cycle loop is nested within the generational cycle loop (see Fig. 5). A single iteration of the reproductive cycle consists of (1) selecting two parent heat exchangers, (2) constructing their respective chromosomes, (3) mating the parents together by combining their genetic material to produce two offspring chromosomes, allowing mutations on the offspring chromosomes to occur, and (4) developing the offspring heat exchangers from their genetic make-up.

Parent heat exchangers are selected for breeding stochastically using the commonly employed roulette wheel algorithm (RWA) discussed by Goldberg [28], in which the probability of a parent being selected is proportional to its calculated fitness.

A single individual heat exchanger can be deconstructed into a chromosome-like structure (genotype), defining that individual's physically observable parameters (phenotype), which will subsequently be subjected to the actions of several genetically inspired operators during the computational breeding process. The complementary process of reconstructing an individual heat exchanger (obtaining its phenotype) from its defining genetic material (its genotype) allows the individual's fitness to then be computed. An individual heat exchanger's chromosome is constructed by coding each of its n defining parameters into a sequence of integers and joining together the n sequences to form a one-dimensional array (see Fig. 6(*a*)). Each element of this chromosomal array may be thought of as a gene having several possible alleles.

Two parent heat exchangers are bred together by first performing a crossover operation on their chromosomes. This operation produces two corresponding offspring chromosomes. To perform the one-point crossover operation, a single cutting point is

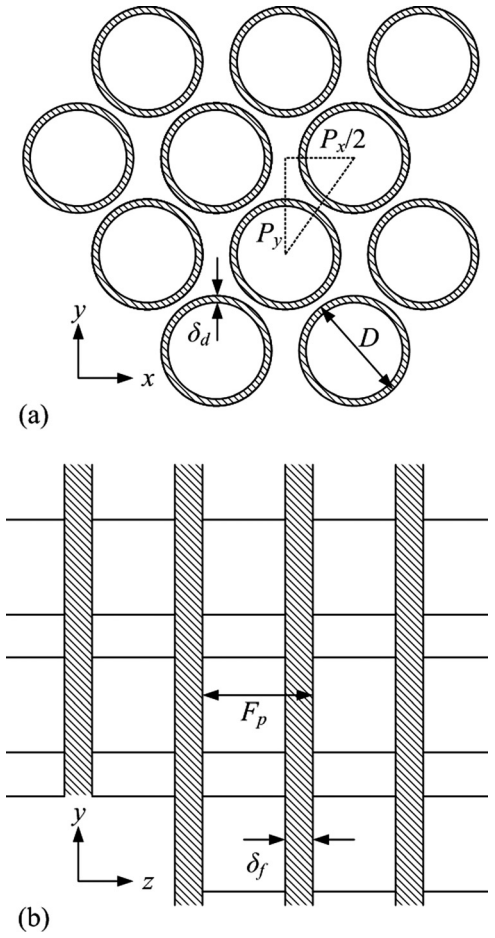

Fig. 4 Geometrical constraints in (*a*) $x-y$ and (*b*) $y-z$ planes

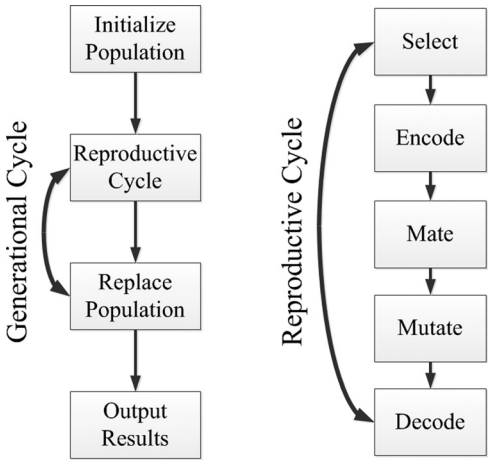

Fig. 5 Visual outline of the basic GA optimizer

randomly selected along the chromosomes, and both parent chromosomes are split here (Fig. 6(*b*)). The chromosomal fragments on one side of the cutting point are interchanged and concatenated to the fragments on the other side (Fig. 6(*c*)), resulting in two offspring chromosomes, whose phenotypes can then be constructed. The crossover operation does not always occur during breeding, occurring at a rate P_C.

Before an offspring chromosome is reconstructed into its corresponding phenotype, however, each gene in the chromosome is subjected to mutation at the rate of P_M. A gene affected by a mutation is replaced by a randomly selected value. Although

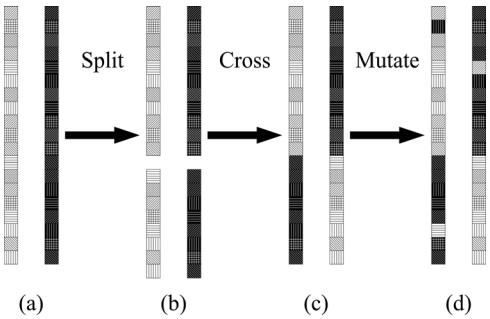

Fig. 6 Schematic of the genetic operators acting during the breeding process. (*a*) Two parent individuals are selected and paired for mating. (*b*) A location on their chromosomes is randomly selected for splitting. (*c*) The crossover mechanism then occurs. (*d*) Subsequently, genetic mutations are allowed to take place.

mutation can destroy a superior offspring, it is necessary to implement in order to preserve variability in the population and to provide a mechanism to overcome premature convergence on secondary maxima in the search space.

In this study, the GA operation parameters are $N_P = 100$, $N_G = 500$, $P_C = 0.90$, and $P_M = 0.05$. A detailed search for the optimal GA operation parameters was not carried out; however, the chosen values are typical, falling within the range typically employed, and perform satisfactorily. Upon completion, the GA optimizer yields $\mathbf{x}^*$ and $F^* = F(\mathbf{x}^*)$, the best solution and its corresponding fitness, respectively.

Results and Discussion

The evolution of the best individual's fitness in each generation is plotted in Fig. 7 for five different trials along with the average of the trials. From this figure, it can be observed that, as generations pass, the computational implementation of natural selection leads to improved heat exchanger designs, as judged by the value of the fitness function. Finally, after N_G generations, the evolution ceases and an optimal, or near-optimal, FTHE is obtained. Running on a 2.20-GHz Intel Core i7-2720QM central processing unit, the average time for the compiled Fortran GA optimization code (with $N_P = 100$ and $N_G = 500$) over the five trials was 15.563 h.

The best solutions $\mathbf{x}^*$ and their corresponding fitness functions $F^* = F(\mathbf{x}^*)$ for the five trials are tabulated in Table 3. As shown in the table, the final fitness functions F^* in the present constrained optimization problem varied only slightly among the five trials, reaching within 6% of the theoretical optimum. However, some of

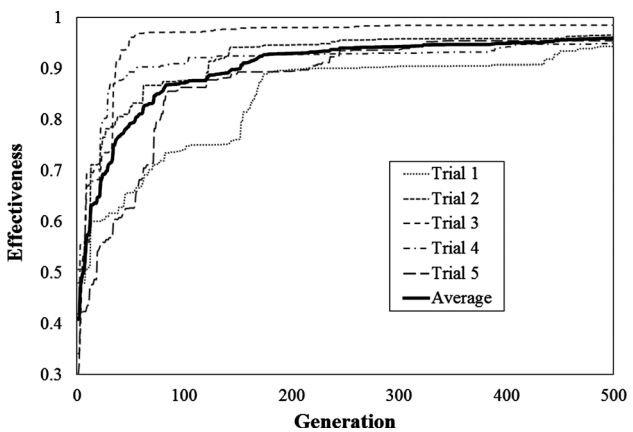

Fig. 7 Fitness evolution of the best individual in each generation for five trials

Table 3 Parameter selection and corresponding fitness for the five trials

		Trial 1	Trial 2	Trial 3	Trial 4	Trial 5
$\mathbf{x}^*$	D (mm)	8.41	7.56	7.34	7.36	8.12
	δ_d (mm)	1.02	3.20	2.95	3.02	1.41
	S_x	1.72	2.74	4.48	4.47	1.41
	S_y	2.23	2.47	1.49	1.03	2.46
	N_x	23	11	5	7	23
	N_y	19	39	47	48	15
	δ_f (mm)	0.50	0.50	0.50	0.51	0.50
	S_z	6.41	4.45	4.87	4.95	4.20
	L_z (mm)	1476	713	1495	1318	1499
	$\dot{m}_1$ (kg s^{-1})	8.01	8.45	13.79	8.40	6.81
F^*	ε	0.94	0.97	0.99	0.95	0.95

the search parameters $\mathbf{x}^*$ varied quite significantly, due to the absence of additional constraints that would decrease the size of the search space. That is, among the five trials, the GA identified nearly equivalent optimums in different regions of the search domain.

The fin thickness and pitch, δ_f and F_p, and tube diameter and pitches, D, P_x, and P_y, together characterize the lower-scale morphology of the fin-side flow (i.e., $\langle m_1 \rangle$ and S_{w_1}) and, along with the mass flow rate $\dot{m}_1$, give rise to the Reynolds number Re_1, which determines the lower-scale fin-side transport coefficients, c_{d_1} and h_1. Similarly, the tube inner diameter and pitches, D_i, P_x, and P_y, characterize the lower-scale morphology of the tube-side flow (i.e., $\langle m_2 \rangle$ and S_{w_2}) and, along with the mass flow rate $\dot{m}_2$, give rise to the Reynolds number Re_2, which determines the lower-scale tube-side transport coefficients, c_{d_2} and h_2. It is the morphology and transport behavior on the lower scale that effects the design of the upper-scale variables, such as the overall exchanger body dimensions, L_x, L_y, and L_z, and the number of tube passes and rows, N_x and N_y (see Fig. 8). As depicted in Fig. 8, the result of Trial 3 is an exchanger characterized by a relatively large face to the air flow, a large number of tube rows N_y, and a small number of tube passes N_x. The tube-side porosity $\langle m_2 \rangle$ and specific surface area S_{w_2} for Trial 3 are relatively low and

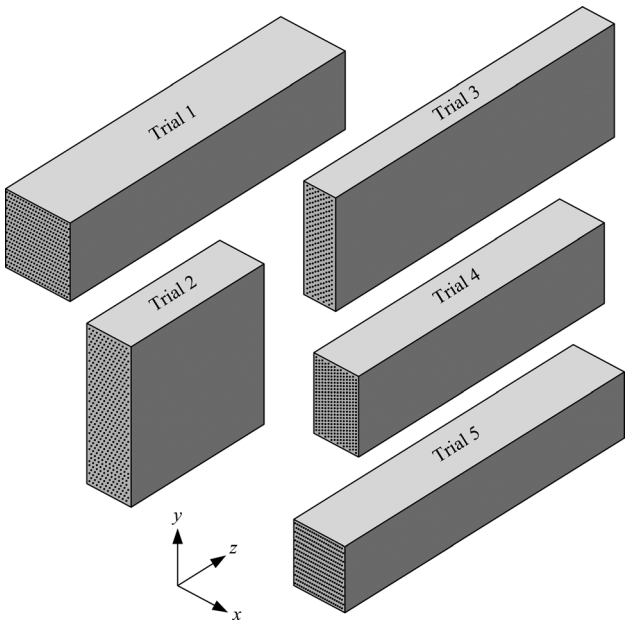

Fig. 8 Optimum heat exchanger body dimensions, L_x, L_y, and L_z, drawn to scale with tube pass and row numbers, N_x and N_y, indicated (tube diameters not drawn to scale) for the five trials

Table 4 Heat exchanger performance at x = x* for the five trials, $\dot{Q}_{max} = 125.58$ kW

Trial	$\dot{Q}$ (kW)	ε (–)	ε_{PP} (–)	$\varepsilon_{\Delta T}$ ($^\circ C^{-1}$)	PP_1 (kW)	PP_2 (kW)	PP_T (kW)	W (kg)	V (m^3)
1	118.54	0.94	2.89	9.62×10^{-2}	40.99	0.07	41.06	297.23	0.1744
2	121.32	0.97	2.02	6.75×10^{-2}	47.51	12.41	59.92	297.93	0.1186
3	123.77	0.99	2.06	6.88×10^{-2}	56.92	3.04	59.96	299.79	0.1265
4	119.34	0.95	2.07	6.89×10^{-2}	52.03	5.74	54.77	296.87	0.1110
5	119.92	0.95	2.02	6.75×10^{-2}	59.03	0.22	59.25	300.00	0.1185

give rise to a relatively high tube-side flow velocity and heat transfer coefficient. The exchanger resulting from Trial 4 shares very similar characteristics with that resulting from Trial 3; however, the number of tube passes N_x is slightly increased and the face area to the air flow is slightly decreased. While the exchanger resulting from Trial 2 is similar in many respects to that resulting from Trials 3 and 4, its length in the z direction is significantly shorter, resulting in a square-shaped face to the air flow. The exchanger resulting from Trial 5, on the other hand, unlike those resulting from Trials 2, 3, and 4, is characterized by a relatively small face to the air flow, a small number of tube rows N_y, and a large number of tube passes N_x. The tube-side porosity $\langle m_2 \rangle$ and specific surface area S_{w_2} are relatively high and give rise to a relatively low tube-side flow velocity and heat transfer coefficient. The exchanger resulting from Trial 1 shares very similar traits with that resulting from Trial 5; however, the number of tube rows N_y is slightly increased. It is interesting to note that, for the five trials, despite the wide variation in tube-side morphology and transport characteristics (between Trials 2, 3, and 4 and Trials 1 and 5), the air side did not see a wide variation in its porosity $\langle m_1 \rangle$, specific surface area S_{w_1}, flow velocity, or heat transfer coefficient.

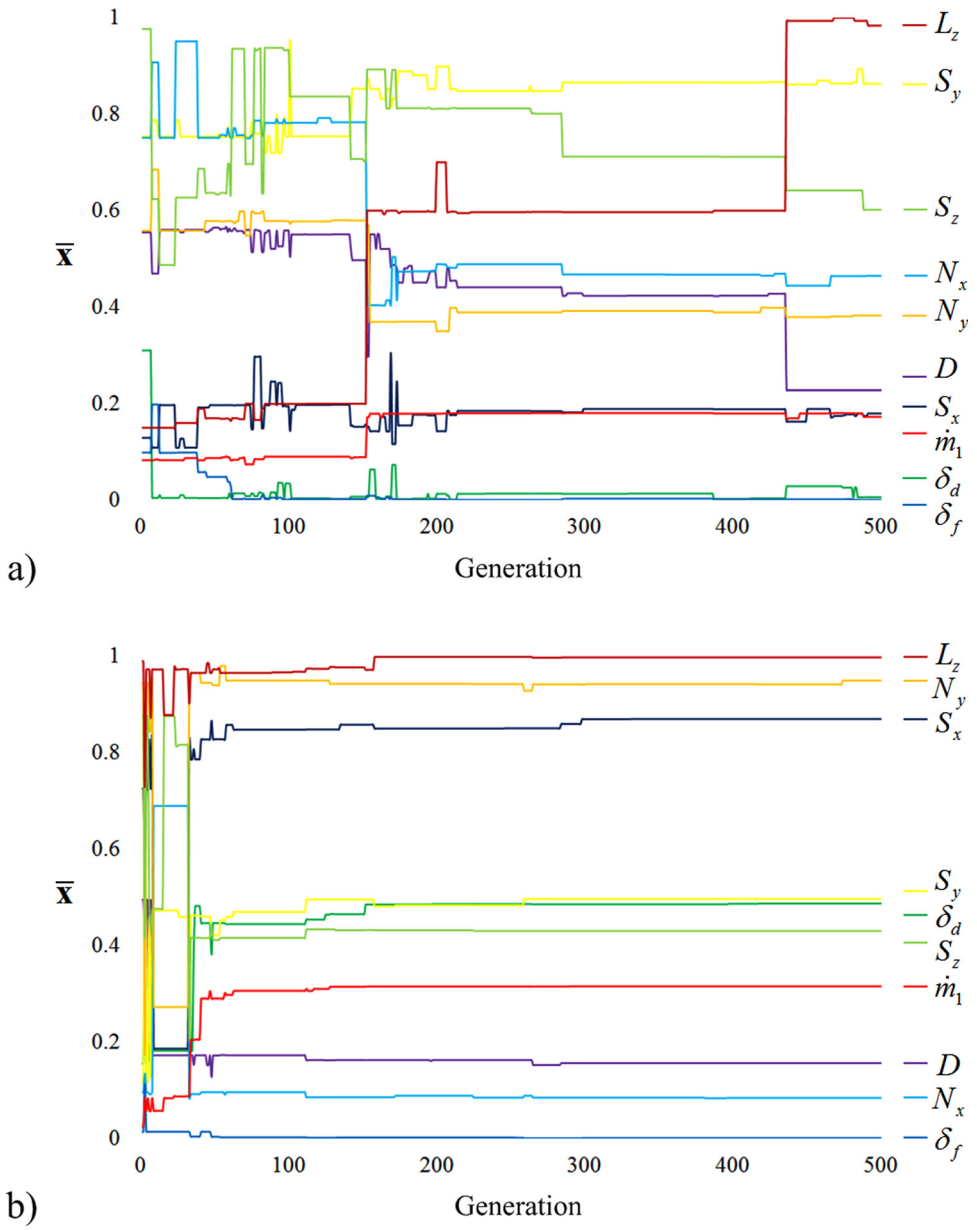

Fig. 9 Evolution of x̄ for the best individual in each generation for (*a*) Trial 1 and (*b*) Trial 3

As was previously discussed, in the present analysis, transport in each of the fluid phases is treated separately from that in the solid phase in order to account for conjugate effects, and it is the lower-scale transport coefficients on each side of the exchanger that connect the transport in the fluid phases to that in the solid phase. In the present study, fin thickness δ_f was minimized in every trial; however, tube-wall thickness δ_d was significantly increased in Trials 2, 3, and 4, relative to Trials 1 and 5, indicating the role that the solid-side effects play in the exchanger design. For example, it is known that, while decreasing the tube-wall thickness reduces the solid-side thermal resistance, increasing it can lead to increased fin-side surface area, thus reducing the overall thermal resistance between the fluids. Such effects must be carefully balanced with other important considerations in the exchanger design, and the present method allows such a balance to be achieved.

In any heat exchanger design process, numerous constraints inevitably arise. Introducing further constraints into the optimization will reduce the size of the search domain until there may be only a single viable solution $\mathbf{x}^*$ remaining. For the successful application of the tool presented here to a specific design problem, constraints must be clearly delineated at the outset by the designer. For example, cost, certain dimensions, and manufacturability constraints all reduce the search domain of the problem. As mentioned above, heat exchanger designers typically select components of their design from a production manual or handbook, and such a finite selection of parameters considerably reduces the design search space. Operational concerns also play a crucial role when specifying constraints. For example, concerns for excessive tube-wall pressure on the tube side and fluid elastic instability [29,30] on the fin side play a prominent role in some heat exchanger designs, and designing to avoid these detrimental phenomena will result in additional constraints. Table 4 tabulates some additional performance parameters of the optimum heat exchangers found at $\mathbf{x}=\mathbf{x}^*$ for the five trials considered in addition to their fitness and includes the presently constrained quantities PP_T and W. It is evident that the heat exchanger optimization procedure was bounded by the imposed constraints on these quantities and that, for nearly every case, these quantities were at or near the constraining values. Thus, constraints play a crucial role in the design process, decreasing the size of the search domain, and must be identified for specific design requirements.

As a final note, variability in convergence speed is evident in Fig. 7. In particular, while Trial 3 converges relatively quickly, Trial 1 converges relatively slowly. Such variability in convergence speed in this study was solely the result of a different initial population and random number seed. Such effects must be carefully considered, and if, unlike the present case, the optimal fitness function value is unknown, a considerable number of function evaluations may be necessary to obtain confidence in a sufficiently near-optimal solution. Due to its computational speed, the VAT-based method presented here allows optimal heat exchangers to be found that could not be obtained with CFD. However, for specific problems, the GA parameters should also be tuned. Domanski et al. [31] presented a study recommending population size and number of generations significantly smaller than those employed here (i.e., $N_P=40$ and $N_G=200$). Implementing these settings or independently finding optimal settings would decrease the computational time further. It is interesting to observe the evolution of the search parameters in parallel to that of the fitness function and to observe the wide range in convergence speed from the perspective of the search parameters. Figure 9 depicts the evolution of the search parameters $\mathbf{x}$ for each generation's best individual in Trial 1 and Trial 3, where the search parameters have been scaled as

$$\bar{\mathbf{x}}=\frac{\mathbf{x}-\mathbf{x}_{\min}}{\mathbf{x}_{\max}-\mathbf{x}_{\min}} \tag{19}$$

and $\mathbf{x}=\mathbf{x}^*$ at the conclusion of the evolution. It is apparent that, while the search parameters in Trial 3 quickly settle on a location in the domain, the search parameters in Trial 1 continue searching throughout the evolution. The difference in convergence speed observed in Figs. 7 and 9 highlights the need for not only careful tuning of the GA parameters but also a fast-running computational method based on the hierarchical modeling methodology presented here.

Conclusion

In this paper, a volume-averaging theory hierarchical model of a finned-tube heat exchanger is presented that provides the basis for an optimization method that enables full exploitation of the possible parameter variations that are known to be beneficial and whose run-time significantly exceeds that of CFD. In the heat exchanger model, convection effects are separated from conduction effects and a conjugate problem is solved, allowing geometric optimization to be performed. The heat exchanger modeling and optimization are based on theoretically correct governing field equations rather than the usual balance equations or ad hoc field equations. This provides a unified design approach based on simultaneous modeling of the thermal hydraulics and thermal structural behavior. This method is easily extended to other heat exchanger surface types. To do so, one only needs to close the VAT-based equations, which amounts to knowing the morphology and transport coefficients for the structure.

A genetic algorithm numerical optimizer is fully integrated with a simulation routine based on the volume-averaging theory model of the finned-tube heat exchanger. Ten parameters describing the finned-tube heat exchanger are simultaneously varied to optimize the heat exchanger's effectiveness, subject to several constraints. Upon completion, the optimization yields an optimized heat exchanger, specifying the selected values of the ten parameters that were varied and the corresponding optimal heat exchanger effectiveness. Such a computational routine provides a valuable and one-of-a-kind tool for heat exchanger designers. Future work can explore new surfaces, integrate other promising optimization methods (e.g., particle swarm optimization, simulated annealing, etc.), and consider multiple-objective optimization methods, (e.g., NSGA-II [32]). Moreover, tube-side phase change, fin-side wet surface conditions, and flexibility in tube circuitry architectures can be incorporated into the model.

Computer-aided numerical simulation, as presented here, cannot yet replace the experimental work, but with the aid of computer calculations, experiments can focus on achieving optimum properties. Model calculations can be used to examine the sensitivity of heterogeneous media performance to key parameters. This minimizes developmental costs and reduces the time required for product commercialization.

Acknowledgment

The support of the DARPA MACE program Grant No. W31P4Q-09-1-0005 is gratefully acknowledged. The views, opinions, and/or findings contained in this article are those of the authors and should not be interpreted as representing the official views or policies, either expressed or implied, of the Defense Advanced Research Projects Agency or the Department of Defense.

Nomenclature

c_d = drag resistance coefficient (–)
c_p = specific heat capacity (J kg^{-1} K^{-1})
D, D_c, D_i = tube outer/collar/inner diameter (m)
D_h = porous media hydraulic diameter (m)
f = friction factor (–)
F = fitness function
h = heat transfer coefficient (W m^{-2} K^{-1})
k = thermal conductivity (W m^{-1} K^{-1})

k_{sT} = effective thermal conductivity of solid phase (W m^{-1} K^{-1})
k_T = turbulent eddy thermal conductivity (W m^{-1} K^{-1})
l = turbulence mixing length (m)
L_x, L_y, L_z = exchanger overall length in x, y, and z directions (m)
$\langle m \rangle$ = local averaged porosity
$\dot{m}$ = mass flow rate (kg s^{-1})
n = number of bounded parameters describing an individual; dimension of the optimization search space
N_G = total number of generations
N_P = total number of individuals in the population; population size
N_x, N_y = columns (x) and rows (y) of tubes
Nu = Nusselt number Nu = (hD_h/k_f)
p = pressure (Pa)
P_C = crossover probability
P_M = mutation probability
P_x, P_y = tube pitch in the air flow (x) and cross-flow (y) directions (m)
PP_1, PP_2 = fin (1) and tube (2) side pumping power (W)
Pr = Prandtl number Pr = (ν_f/α_f)
$\dot{Q}$ = total heat transfer rate (W)
$\dot{Q}_1, \dot{Q}_2$ = fin (1) and tube (2) side total heat transfer rate (W)
$\dot{Q}_{\max}$ = maximum heat transfer rate $\dot{Q}_{\max} = \dot{m}_2 c_{p_2}(T_{2,\text{in}} - T_{1,\text{in}})$ (W)
Re = Reynolds number Re = $(\rho_f \tilde{u} D_h/\mu_f)$
S_w = local specific surface area $\partial S_w/\Delta\Omega$ (m^{-1})
S_x, S_y = tube pitch in the air flow (x) and cross flow (y) directions, scaled with tube outer diameter
S_z = fin pitch over fin thickness
T = temperature (K)
u, v, w = velocity in x, y, z directions (m s^{-1})
V = heat exchanger total volume (m^3)
W = heat exchanger total mass (kg)
$\mathbf{x}$ = search space vector
∂S_w = internal surface area in the REV (m^2)

Greek Symbols

α = thermal diffusivity (m^2 s^{-1})
δ_d = tube wall thickness (m)
δ_f = fin thickness (m)
$\Delta\Omega$ = representative elementary volume (REV) (m^3)
ε = heat exchanger effectiveness $\varepsilon = \dot{Q}_1/\dot{Q}_{\max}$
ε_{PP} = alternate effectiveness $\varepsilon_{PP} = \dot{Q}_1/PP_T$
$\varepsilon_{\Delta T}$ = alternate effectiveness $\varepsilon_{\Delta T} = \varepsilon_{PP}/(T_{2,\text{in}} - T_{1,\text{in}})$ (K^{-1})
μ = dynamic viscosity (kg m^{-1} s^{-1})
ν = kinematic viscosity (m^2 s^{-1})
ρ = density (kg m^{-3})

Subscripts

avg = average
f = fluid phase
in/out = inlet/outlet condition
L = laminar
s = solid phase
tot = total
T = turbulent
1 = air/fin side
2 = water/tube side
max = maximum
min = minimum

Superscripts

$\tilde{}$ = value in fluid phase averaged over the REV
$-$ = mean turbulent quantity; scaled quantity
$'$ = turbulent fluctuation quantity
$*$ = optimum

References

[1] Ozkol, I., and Komurgoz, G., 2005, "Determination of the Optimum Geometry of the Heat Exchanger Body Via a Genetic Algorithm," Numer. Heat Transfer, Part A, **48**(3), pp. 283–296.
[2] Xie, G., Wang, Q., and Sunden, B., 2008, "Application of a Genetic Algorithm for Thermal Design of Fin-and-Tube Heat Exchangers," Heat Transfer Eng., **29**(7), pp. 597–607.
[3] Domanski, P. A., 1989, "EVSIM: An Evaporator Simulation Model Accounting for Refrigerant and One Dimensional Air Distribution," Department of Energy Report No. NISTIR 89-4133, p. 142.
[4] NIST, 2003, *EVAP-COND-Simulation Models for Finned-Tube Heat Exchangers*, NIST, Gaithersburg, MD.
[5] Domanski, P. A., and Yashar, D., 2007, "Optimization of Finned-Tube Condensers Using an Intelligent System," Int. J. Refrig., **30**(3), pp. 482–488.
[6] Jiang, H., Aute, V., and Radermacher, R., 2006, "CoilDesigner: A General-Purpose Simulation and Design Tool for Air-to-Refrigerant Heat Exchangers," Int. J. Refrig., **29**(4), pp. 601–610.
[7] Abdelaziz, O., Aute, V., Azarm, S., and Radermacher, R., 2010, "Approximation-Assisted Optimization for Novel Compact Heat Exchanger Designs," HVAC&R Res., **16**(5), pp. 707–728.
[8] Mousavi, S. S., Hooman, K., and Mousavi, S. J., 2007, "Genetic Algorithm Optimization for Finned Channel Performance," Appl. Math. Mech., **28**(12), pp. 1597–1604.
[9] Mousavi, S. S., and Hooman, K., 2006, "Heat and Fluid Flow in Entrance Region of a Channel With Staggered Baffles," Energy Convers. Manage., **47**(15–16), pp. 2011–2019.
[10] Matos, R. S., Laursen, T. A., Vargas, J. V. C., and Bejan, A., 2004, "Three-Dimensional Optimization of Staggered Finned Circular and Elliptic Tubes in Forced Convection," Int. J. Thermal Sci., **43**(5), pp. 477–487.
[11] Fabbri, G., 2000, "Heat Transfer Optimization in Corrugated Wall Channels," Int. J. Heat Mass Transfer, **43**(23), pp. 4299–4310.
[12] Foli, K., Okabe, T., Olhofer, M., Jin, Y., and Sendhoff, B., 2006, "Optimization of Micro Heat Exchanger: CFD, Analytical Approach and Multi-Objective Evolutionary Algorithms," Int. J. Heat Mass Transfer, **49**(5–6), pp. 1090–1099.
[13] Hilbert, R., Janiga, G., Baron, R., and Thévenin, D., 2006, "Multi-objective Shape Optimization of a Heat Exchanger Using Parallel Genetic Algorithms," Int. J. Heat Mass Transfer, **49**(15–16), pp. 2567–2577.
[14] Hooman, K., and Gurgenci, H., 2010, "Porous Medium Modeling of Air-Cooled Condensers," Transp. Porous Media, **84**(2), pp. 257–273.
[15] Catton, I., 2011, "Conjugate Heat Transfer Within a Heterogeneous Hierarchical Structure," ASME J. Heat Transfer, **133**(10), p. 103001.
[16] Travkin, V. S., and Catton, I., 2001, "Transport Phenomena in Heterogeneous Media Based on Volume Averaging Theory," *Advances in Heat Transfer*, G. G. Hari, and A. H. Charles, eds., Elsevier, New York, pp. 1–144.
[17] Whitaker, S., 1967, "Diffusion and Dispersion in Porous Media," AIChE J., **13**(3), pp. 420–427.
[18] Whitaker, S., 1986, "Flow in Porous Media II: The Governing Equations for Immiscible, Two-Phase Flow," Transp. Porous Media, **1**(2), pp. 105–125.
[19] Whitaker, S., 1986, "Flow in Porous Media I: A Theoretical Derivation of Darcy's Law," Transp. Porous Media, **1**(1), pp. 3–25.
[20] Shcherban, A. N., Primak, A. V., and Travkin, V. S., 1986, "Mathematical Models of Flow and Mass Transfer in Urban Roughness Layer," Problemy Kontrolya i Zaschita Atmosfery or Zagryazneniya, **12**, pp. 3–10.
[21] Primak, A. V., Shcherban, A. N., and Travkin, V. S., 1986, "Turbulent Transfer in Urban Agglomerations on the Basis of Experimental Statistical Models of Roughness Layer Morphological Properties," Trans. World Meteorological Org. Conf. on Air Pollution Modelling and its Application, WMO, Geneve, Switzerland, pp. 259–266.
[22] Travkin, V., and Catton, I., 1992, *Models of Turbulent Thermal Diffusivity and Transfer Coefficients for a Regular Packed Bed of Spheres*, Vol. 193, ASME, New York, p. 15.
[23] Travkin, V. S., Catton, I., and Gratton, L., 1993, *Single Phase Turbulent Transport in Prescribed Non-Isotropic and Stochastic Porous Media*, Vol. 240, ASME, New York, p. 43.
[24] Wang, C.-C., Chi, K.-Y., and Chang, C.-J., 2000, "Heat Transfer and Friction Characteristics of Plain Fin-and-Tube Heat Exchangers—Part II: Correlation," Int. J. Heat Mass Transfer, **43**(15), pp. 2693–2700.
[25] Zhou, F., Hansen, N. E., Geb, D. J., and Catton, I., 2011, "Obtaining Closure for Fin-and-Tube Heat Exchanger Modeling Based on Volume Averaging Theory (VAT)," ASME J. Heat Transfer, **133**(11), p. 111802.
[26] Techo, R., Tickner, R. R., and James, R. E., 1965, "An Accurate Equation for the Computation of the Friction Factor for Smooth Pipes for the Reynolds Number," ASME J. Appl. Mech., **32**, p. 443.
[27] Whitaker, S., 1972, "Forced Convection Heat Transfer Correlations for Flow in Pipes, Past Flat Plates, Single Cylinders, Single Spheres, and for Flow in Packed Beds and Tube Bundles," AIChE J., **18**(2), pp. 361–371.
[28] Goldberg, D. E., 1989, *Genetic Algorithms in Search, Optimization, and Machine Learning*, Addison-Wesley, Reading, MA.
[29] Chen, S. S., and Jendrzejcyk, J. A., 1981, "Experiments on Fluid Elastic Instability in Tube Banks Subjected to Liquid Cross Flow," J. Sound Vib., **78**(3), pp. 355–381.

[30] Weaver, D. S., and Grover, L. K., 1978, "Cross-Flow Induced Vibrations in a Tube Bank—Turbulent Buffeting and Fluid Elastic Instability," J. Sound Vib., **59**(2), pp. 277–294.
[31] Domanski, P. A., Yashar, D., Lee, S., and Wojtusiak, J., 2011, "Practical Aspects of Applying Evolutionary Algorithms for Optimizing Refrigerant Circuitry in Heat Exchangers," 23rd IIR International Congress of Refrigeration, Prague, p. 8.
[32] Deb, K., Pratap, A., Agarwal, S., and Meyarivan, T., 2002, "A Fast and Elitist Multiobjective Genetic Algorithm: NSGA-II," IEEE Trans. Evol. Comput., **6**(2), pp. 182–197.